# Weierstraß-Institut
## für Angewandte Analysis und Stochastik
### Leibniz-Institut im Forschungsverbund Berlin e. V.

Preprint ISSN 2198-5855


# Consequences of uncertain friction for the transport of natural gas through passive networks of pipelines


Holger Heitsch, Nikolai Strogies



submitted: June 14, 2018



Weierstrass Institute
Mohrenstr. 39
10117 Berlin
Germany
E-Mail: holger.heitsch@wias-berlin.de



No. 2513
Berlin 2018



2010 *Mathematics Subject Classification.* 60J10, 90B15, 90C15.

*Key words and phrases.* Uncertainty quantification, semilinear systems of balance laws, Markov chain Monte Carlo, reliability of gas networks, nomination validation, spheric-radial decomposition.

This work is supported by the German Research Foundation (DFG) within the projects B02 and B04 of CRC TRR 154.

Edited by
Weierstraß-Institut für Angewandte Analysis und Stochastik (WIAS)
Leibniz-Institut im Forschungsverbund Berlin e. V.
Mohrenstraße 39
10117 Berlin
Germany

Fax: +49 30 20372-303
E-Mail: preprint@wias-berlin.de
World Wide Web: http://www.wias-berlin.de/

# Consequences of uncertain friction for the transport of natural gas through passive networks of pipelines

Holger Heitsch, Nikolai Strogies

**Abstract**

Assuming a pipe-wise constant structure of the friction coefficient in the modeling of natural gas transport through a passive network of pipes via semilinear systems of balance laws with associated linear coupling and boundary conditions, uncertainty in this parameter is quantified by a Markov chain Monte Carlo method. Here, information on the prior distribution is obtained from practitioners. The results are applied to the problem of validating technical feasibility under random exit demand in gas transport networks. In particular, the impact of quantified uncertainty to the probability level of technical feasible exit demand situations is studied by two example networks of small and medium size. The gas transport of the network is modeled by stationary solutions that are steady states of the time dependent semilinear problems.

## 1 Introduction

The transport of natural gas through a single pipe can be modeled by a simplification of the full Euler equations, describing the conservation of mass as well as balance of momentum and energy in fluid dynamics. An overview on existing models for transport of natural gas can be found in [6] and we employ the notation of this work. Assuming a heat flux through the pipe walls compensating discontinuities of temperature in case of shock- and rarefaction waves, energy is no longer a balanced quantity (see [20, Section 14.6]). Working under such a regime, an associated system approximately describing the underlying physics is given by the fully nonlienar system of balance laws

$$\begin{aligned} \rho_t + q_x &= 0, \\ q_t + (p(\rho) + \tfrac{q^2}{\rho})_x &= \lambda \tfrac{q|q|}{\rho} - g\rho h', \end{aligned} \tag{ISO 1}$$

which is a well known model for gas transport, see, e.g., [5, 12, 17]. Here, $\rho, q, g, h'$ denote density, volume flow, gravitational constant and slope of the pipe, respectively. Further, $p(\rho)$ represents the pressure depending on the density of the natural gas, usually described by an equation of state, and $\lambda$ is the friction coefficient, also known as Darcy friction factor, quantifying the influence of friction at the pipe wall on the flow behavior. A priory, the friction coefficient is assumed to be a function of the spatial position accounting for local effects in the internal coating of the pipe or local changes in the diameter caused by pollution.

Assuming additional simplifications in (ISO 1), like considering only planar networks with $h' \equiv 0$, neglecting the influence of $\frac{q^2}{\rho}$ in the flux term and utilizing the simplified pressure law $p(\rho) = a^2\rho$, where

DOI 10.20347/WIAS.PREPRINT.2513 Berlin 2018

$a > 0$ denotes the constant speed of sound, we obtain a semilinear system of first-order partial differential equations. Defined on a pipe which is represented by the interval $(x_L, x_R)$ with $x_L < x_R$, it is given by

$$\begin{aligned} \rho_t + q_x &= 0, \\ q_t + a^2 \rho_x &= -\lambda \frac{q|q|}{\rho}, \end{aligned} \qquad \text{on } (0,T) \times (x_L, x_R), \tag{ISO 2}$$

where $T > 0$ represents the time horizon. A brief discussion of the above mentioned simplifications can be found in [12, 22]. To obtain a well posed forward problem, we in addition consider the initial conditions

$$\rho(0,\cdot) = \rho_0(\cdot), \quad q(0,\cdot) = q_0(\cdot) \text{ for } x \in (x_L, x_R), \tag{IC}$$

and boundary conditions. System (ISO 2) is strictly hyperbolic with one strictly negative and one strictly positive eigenvalue. Consequently, conditions on linear combinations of the state variables $\rho$ and $q$ are required at both ends of the pipe. In other words, there have to exist certain vectors $c_L, c_R \in \mathbb{R}^2$ and functions $d_L, d_R \in L^\infty(0,T)$ such that

$$c_L^\top(\rho(t,x_L), q(t,x_L)) = d_L(t), \quad c_R^\top(\rho(t,x_R), q(t,x_R)) = d_R(t). \tag{BC}$$

Besides the time-dependent models, a stationary model is considered as well, where the boundary data are constant. It is obtained by neglecting the time derivatives in system (ISO 2). The resulting ordinary differential equations

$$q_x = 0, \quad \rho_x = -\tfrac{\lambda}{a^2} \tfrac{q|q|}{\rho},$$

with associated initial conditions $q(x_L) = q$, $\rho(x_L) = \rho$ that are obtained from the original boundary conditions, can be solved explicitly, providing

$$q(x) \equiv q, \quad \rho(x) = \sqrt{\rho(x_L)^2 - 2\bar{\lambda}(x)\tfrac{q|q|}{a^2}} \tag{ISO-ALG}$$

with $\bar{\lambda}(x) = \int_{x_L}^{x} \lambda(\tau) d\tau$. Note that the initial conditions can be imposed at arbitrary spatial positions along the pipe. In particular, data for volume flow and density do not necessarily have to be imposed at the same position.

In the context of obtaining information on the friction coefficient out of measurements, for example, measurements of pressure at certain points in the network, the Bayesian framework is based on the uncertainty-to-observation operator $\mathcal{G}$ which maps the underlying unknown (the friction coefficient) onto the measurement data $y$. It represents a composition of the solution operator associated to the underlying PDE problem (ISO 2), extended to a passive network as discussed below, applied to the coefficient $\lambda$ and a data formation operator. In case of density being measured at finitely many points in time $t_j \in [0,T], j = 1, ..., K$, and at a position $\bar{x}$ within the network, we consider

$$\mathcal{G}(\lambda) = (\rho(t_1, \bar{x}), ..., \rho(t_K, \bar{x}))^\top. \tag{1}$$

Since the measuring process introduces errors to the observation, we find

$$y = \mathcal{G}(\lambda) + \eta \Leftrightarrow \eta = y - \mathcal{G}(\lambda), \tag{2}$$

with $\eta \in \mathbb{R}^K$ denoting the measurement error. In the work at hand, we assume this error to be Gaussian noise with mean zero, associated covariance matrix $\Gamma \in R^{K\times K}$ and probability density function (PDF) denoted by $\pi_{DL}$. Given a friction coefficient $\lambda$, the probability of obtaining measurement data y is given according to

$$P(y|\lambda) = \pi_{DL}(y - \mathcal{G}(\lambda)), \tag{3}$$

also called likelihood of the data. Now, using Bayes' theorem, we can incorporate available "prior" knowledge on $\lambda$ and provide its probability, given the measured data $y$, as

$$P(\lambda|y) \propto P(y|\lambda)P(\lambda). \tag{4}$$

Our knowledge on the distribution of $\lambda$, i.e., $P(\lambda)$, is called prior and the probability of $\lambda$ given the data y, i.e., $P(\lambda|y)$, is called posterior. Both probability distributions are equipped with associated PDF's $\pi_{PR}$ and $\pi_{PO}$.

The Bayesian approach to inverse problems involving a partial differential equation has been intensively studied in the last years. For an overview we refer to [2] and the references therein. In particular we mention [4], where a Multi-Level Markov chain Monte Carlo method has been investigated that allows for incorporating mesh-refinement strategies for the partial differential equation. To the best of our knowledge, besides the investigations in [13, 18], where the first one merely considers a single pipe while allowing for a spatially distributed friction coefficient and the latter one not employing the Bayesian approach, obtaining information on distributions of the friction coefficient has not been subject of investigation so far.

# 2 Results for the state equations

This section is dedicated to discussions on notions of solutions for the underlying system in both the time independent and dependent setting and the extension of the respective ordinary, and partial differential equations to passive networks of pipelines.

## 2.1 Steady states

As outlined above, the time independent model of gas flow results in an algebraic solution representing the connection between density and flow along a pipe as described in (ISO-ALG). As consequence, in a passive gas network there exists a explicit characterization of gas flow feasibility that is based on the algebraic formulation of mass and momentum conservation, respectively, the Kirchhoff's first and second law. Feasibility of gas load (or nomination) is equivalent to the existence of a pressure-flow profile fulfilling that Kirchhoff's laws and meeting nodal bounds on the pressure. For a characterization of the

set of all capacities that can be realized, functional relations in the nomination space are sought, that hold if and only if the nomination is feasible. These functional relations become closer and closer coupled among each other the more intertwined cycles there are in the network. In what follows, a general characterization is derived that still contains as many implicit indeterminates as there are fundamental cycles in the network.

The gas transportation network is considered as a connected directed graph $G = (\mathcal{V}, \mathcal{E})$, with $|\mathcal{V}| = n + 1$ nodes and $|\mathcal{E}| = m \geq n$ edges. Assume the network is in steady state let be $q \in \mathbb{R}^m$ the flow along the edges of $G$ and $(p_0, p) \in \mathbb{R}^{n+1}$ the pressure at nodes in $\mathcal{V}$. The network topology let be given by $\mathcal{I} \in \mathbb{R}^{n\times m}$, a reduced node-arc incidence matrix of $G$. Inflows and outflow are described by a balanced load vector $(b_0, b) \in \mathbb{R}^{n+1}$, i.e., it holds $-\mathbb{1}^\top b = b_0$, where $\mathbb{1}$ denotes the vector of all ones in suitable dimension, here $n$. Moreover, we make the sign convention that $b_i \leq 0$ at injection points (entries) and $b_i \geq 0$ at withdrawal points (exits). Mass, or mass flow, conservation at each node in $\mathcal{V}$ (Kirchhoff's first law) now reads

$$\mathcal{I}q \;=\; b. \tag{5}$$

Denoting with $o(e) \in \mathcal{V}$ and $\pi(e) \in \mathcal{V}$ the origin and head of some edge $e \in \mathcal{E}$, respectively, then the pressure drop between the ends of pipe $e \in \mathcal{E}$ causes a constant flow along the pipe due to the condition (Kirchhoff's second law)

$$(p_k)^2 \;-\; (p_\ell)^2 \;=\; \Lambda_e |q_e| q_e, \tag{6}$$

where $k = o(e)$ and $\ell = \pi(e)$. The latter equation is equivalent to (ISO-ALG), but formulated in terms of pressure values rather than density right now. Here, the the so-called *roughness* coefficient $\Lambda_e$ combines constant parameters and the integral friction coefficient $\lambda_e$ of some pipe $e \in \mathcal{E}$. In particular, with the law $p = a^2\rho$ we have

$$\Lambda_e = \Lambda_e(\lambda_e) = 2a^2 l_e \lambda_e, \tag{7}$$

where $l_e$ denotes the length of pipe $e$, and $a$ is the speed of sound again. With technical lower and upper pressure limits $p^{min}, p^{max}$ we are led to introduce the following set $M_{feas}$ of *feasible load (nomination) vectors*.

**Definition 1.** *A load vector $(b_0, b)$ is feasible load vector, if and only if $(b_0, b)$ is contained in the feasibility set $M_{\mathrm{feas}}$ defined as*

$$M_{\mathrm{feas}} := \left\{ (b_0, b) \;\middle|\; -\mathbb{1}^\top b = b_0;\; \exists (q, p) \text{ with } p \in \left[p^{min}, p^{max}\right] \text{ and } (5), (6) \right\}. \tag{8}$$

The following provides a characterization of the set $M_{\mathrm{feas}}$, where all pressure variables and "most of" the flow variables are eliminated. With the notation $\Lambda := \mathrm{diag}\{\Lambda_e \,|\, e \in \mathcal{E}\}$ for roughness, from [11] we take the following result.

**Theorem 1** ([11, Theorem 1])**.** *Let $\mathcal{I} = (\mathcal{I}_B, \mathcal{I}_N)$ be a partition into basis and nonbasis submatrices of the incidence matrix $\mathcal{I}$. Let $\Lambda_B, \Lambda_N$ and $q_B, q_N$ be according partitions of $\Lambda$ and $q$. Define*

$$h : \mathbb{R}^n \times \mathbb{R}^{|N|} \to \mathbb{R}^n,\; h(u, v) \;:=\; \left(\mathcal{I}_B^\top\right)^{-1} \Lambda_B \left|\mathcal{I}_B^{-1}(u - \mathcal{I}_N v)\right| \left(\mathcal{I}_B^{-1}(u - \mathcal{I}_N v)\right). \tag{9}$$

*Then,* $M_{\mathrm{feas}}$ *consists of all* $(b_0, b)$ *with* $-\mathbb{1}^\top b = b_0$ *for which there is a* $z \in \mathbb{R}^{|N|}$ *such that*

$$\begin{aligned}
\mathcal{I}_N^\top h(b,z) &= \Lambda_N |z| z && (10)\\
(p_0^{min})^2 &\le \min_{k=1,\dots,n} \left[(p_k^{max})^2 + h_k(b,z)\right] && (11)\\
(p_0^{max})^2 &\ge \max_{\ell=1,\dots,n} \left[(p_\ell^{min})^2 + h_\ell(b,z)\right] && (12)\\
\min_{k=1,\dots,n} \left[(p_k^{max})^2 + h_k(b,z)\right] &\ge \max_{\ell=1,\dots,n} \left[(p_\ell^{min})^2 + h_\ell(b,z)\right]. && (13)
\end{aligned}$$

Up to finding an auxiliary variable $z$ satisfying (10), Theorem 1 identifies fully explicit feasibility conditions with respect to the load vector $(b_0, b)$ and the side constraints (pressure bounds). Therefore, the feasibility test for balanced $(b_0, b)$ reduces to determining the unique $z$ solving (10) and then checking the inequality system (11), (12), (13). Observe that the dimension of $z$ corresponds to the number of columns of the nonbasis part $\mathcal{I}_N$ of the reduced incidence matrix $\mathcal{I}$, hence to the number of fundamental cycles in the network. Obviously, the situation should be particularly comfortable for networks without cycles, as is illustrated now.

**Special case of tree networks**

Suppose $G = (\mathcal{V}, \mathcal{E})$ is a tree (trivially a spanning tree of itself). Fix an arbitrary leaf node as root and number it by $0$. Direct all edges in $\mathcal{E}$ away from the root. The incidence matrix $\mathcal{I}$ of $G$ already is the basis matrix $\mathcal{I}_B$ so that there is no nonbasis portion $\mathcal{I}_N$. Using depth-first search, number the nodes so that numbers increase along any path from the root to one of the leaves. For $k, \ell \in \mathcal{V}$, denote $k \succeq \ell$ if, in $G$, the unique directed path from the root to $k$, denoted $\Pi(k)$, passes through $\ell$. Since $\mathcal{I}_N$ vacuous and $\Lambda = \Lambda_B$, one obtains for $h$ as defined in (9)

$$h(b,z) \;=\; h(b) \;=\; \left(\mathcal{I}^{-1}\right)^\top \Lambda \left|\mathcal{I}^{-1} b\right| \left(\mathcal{I}^{-1} b\right)$$

and componentwise, for $k = 1, \dots, n$, and emphasizing the implicit dependency of the friction coefficients $\lambda_e$ according to (7),

$$h_k(b,\lambda) \;=\; \sum_{e \in \Pi(k)} 2a^2 l_e \lambda_e \left| \sum_{t \in \mathcal{V}, t \succeq \pi(e)} b_t \right| \left( \sum_{t \in \mathcal{V}, t \succeq \pi(e)} b_t \right), \qquad k = 0, \dots, n, \tag{14}$$

as shown in [11]. To reduce technicality we assume that the network has the node $0$ as the only entry and all remaining nodes as exits, again with all edges directed away from $0$. Then in (14) flow and edge directions conform, leading to

$$h_k(b,\lambda) = \sum_{e \in \Pi(k)} 2a^2 l_e \lambda_e \left( \sum_{t \in \mathcal{V}, t \succeq \pi(e)} b_t \right)^2, \qquad k = 0, \dots, n. \tag{15}$$

Now, Theorem 1 specializes as follows:

**Corollary 1.** *If the network is a tree with a single entry as its root, then the set of feasible load vectors is given by*

$$M_{\text{feas}} = \left\{ (-\mathbb{1}^\top b, b) \,\middle|\, 0 \leq \min_{k=0,\dots,n} \left\{ (p_k^{max})^2 + h_k(b,\lambda) \right\} - \max_{\ell=0,\dots,n} \left\{ (p_\ell^{min})^2 + h_\ell(b,\lambda) \right\} \right\}, \quad (16)$$

*where $h_k(b,\lambda)$, $k = 0,\dots,n$, is as in (15). Note that $h_0(\cdot,\cdot) \equiv 0$ here.*

## 2.2 Time dependent problems

The state system (ISO 2) can be written as

$$y_t + Ay_x = g(y), \quad (17)$$

with $y := (\rho, q)^\top$ denoting the state vector. Here $g(y)$ and the $A$ are defined by

$$g(y) = (0, -\lambda \tfrac{q|q|}{\rho})^\top \text{ and } A = \begin{pmatrix} 0 & 1 \\ a^2 & 0 \end{pmatrix}.$$

The eigenvalues of $A$, given by $\sigma_1 = -a < a = \sigma_2$, define *characteristic lines*. Indeed, given a position $x \in (x_L, x_R)$ and a point in time $\tau \in (0,T)$, the characteristics passing through $(\tau, x)$ are defined as solutions to the ordinary differential equations

$$\dot{s}_i(t;\tau,t) = \sigma_i$$

with $s_i(\cdot;\tau,x) : \mathbb{R} \to \mathbb{R}$ satisfying $s_i(\tau;\tau,x) = (\tau,x)$. The index $i$ relates characteristic and eigenvalue. Since the domain $\mathcal{Q}$ is bounded, we define the times $\underline{t}_i(\tau,x) \in [0,\tau]$ and $\bar{t}_i(\tau,x) \in [\tau,T]$, specifying the time, the $i$-th characteristic passing through $(\tau,x)$ satisfies $(t, s_i(t;\tau,x)) \in \mathcal{Q}$, i.e., we either have $s_i(\underline{t}_i(\tau,x);\tau,x) = x$, $x \in [x_L,x_R]$, in case the characteristic intersects with $\{0\} \times [x_L,x_R]$ or $s_1(\underline{t}_1(\tau,x);\tau,x) = x_R$ or $s_2(\underline{t}_2(\tau,x);\tau,x) = x_L$ if the characteristic intersects with the boundary $(0,T) \times \{x_R\}$ or $(0,T) \times \{x_L\}$, respectively. The time $\bar{t}_i(\tau,x)$ is defined correspondingly. Once more, the value $a$ represents the speed of sound in the model, i.e., the speed information is propagated with through the spatial domain.

Based on a transformation of the representation (17), we consider *broad solutions* for (ISO 2) as follows. Due to strict hyperbolicity of (ISO 2), there exist a matrix $L \in \mathbb{R}^{n\times n}$ such that $A = LDL^{-1}$ where $D = \operatorname{diag}(\sigma_i) \in \mathbb{R}^{2\times 2}$. Multiplying (17) from the left by $L^{-1}$, using the linearity of differentiation and setting $\mathcal{T}(y) := L^{-1}y$ and $f(y) := L^{-1}g(y)$, we obtain

$$(\mathcal{T}(y))_t + D(\mathcal{T}(y))_x = f(y),$$

a system of scalar, linear transport equations, merely coupled by the source term on the right hand side. Given (ISO 2), the transformation matrices are

$$L = c_a \begin{pmatrix} 1 & 1 \\ -a & a \end{pmatrix}, \quad L^{-1} = (2c_a)^{-1} \begin{pmatrix} 1 & -a^{-1} \\ 1 & a^{-1} \end{pmatrix}.$$

Also note that the linear transport equations even have constant coefficients. In case of a single equation of this type, it is well known that solutions are described by ordinary differential equations along the characteristic line, defined by the constant coefficient. The concept of broad solutions extends this property to systems in that the transformed components of $\mathcal{T}(y)$ are absolutely continuous functions along the corresponding characteristic lines. Broad solutions to semilinear systems of balance laws for unbounded domains have been studied for example in [1, 21], while in [14, 15] bounded domains have been considered. We recall the definition from [18] as follows.

**Definition 2.** *A broad solution of* (ISO 2) *is a function $y = L\mathcal{T}(y) : \mathcal{Q} \to \mathbb{R}^2$ such that, for almost every $(\tau, x) \in \mathcal{Q}$, the map $t \mapsto \mathcal{T}_i(y)[t, s_i(t;\tau,x)]$ is an absolutely continuous function satisfying*

1 *at almost every $(\tau, x) \in \mathcal{Q}$ the ordinary differential equations*

$$\frac{d}{dt}\mathcal{T}_i(y)[t, s_i(t;\tau,x)] = f_i(t, s_i(t;\tau,x), y(t, s_i(t;\tau,x))) \tag{18}$$

*almost everywhere on $(\underline{t}_i(\tau,x), \bar{t}_i(\tau,x))$ for $i = 1, 2$,*

2 *the initial condition at $x \in (x_L, x_R)$*

$$\mathcal{T}_i(y)[0, x] = c_i y_0(x),$$

3 *the boundary condition at $x_L$ in the sense that for almost every $t \in (0, T)$ we have*

$$\mathcal{T}_2(y)[t, x_L] = c_2 C_L^{-1} \begin{pmatrix} \mathcal{T}_1(y)[t, x_L] \\ d_L(t) \end{pmatrix},$$

4 *the boundary condition at $x_R$ in the sense that for almost every $t \in (0, T)$ we have*

$$\mathcal{T}_1(y)[t, x_R] = c_1 C_R^{-1} \begin{pmatrix} \mathcal{T}_2(y)[t, x_R] \\ d_R(t) \end{pmatrix},$$

5 *in case of a network, 1 and 2 hold true on all pipes of the network, 3 and 4 are satisfied at entry- and exit nodes (cf. Sect. 2.1), and in addition, coupling conditions* (20) *and* (21) *are satisfied at interior nodes (nodes with no consumption) of the network.*

The lateral boundaries of $\mathcal{Q}$ are approached by exactly one of the characteristics for every $t \in (0, T)$. To be able to reconstruct the original variables at the boundary, the matrices

$$C_L = \begin{pmatrix} c_1 \\ c_L \end{pmatrix}^\top, \quad C_R = \begin{pmatrix} c_2 \\ c_R \end{pmatrix}^\top$$

have to be invertible, restricting the possible linear combinations of $y$ that can be prescribed. Here, $c_1, c_2 \in \mathbb{R}^2$ denote the rows of $L^{-1}$.

As it can be seen in [18, Proposition 2], solutions as in (ISO-ALG) (corresponding to Definition 1 in Sect. 2.1) form steady states for the time dependent problem (ISO 2) in the sense of Definition 2.

The coupling conditions (20) and (21) allow for reconstructing the original state variables from the transformed variables $\mathcal{T}^{(i)}$ as the following example demonstrates.

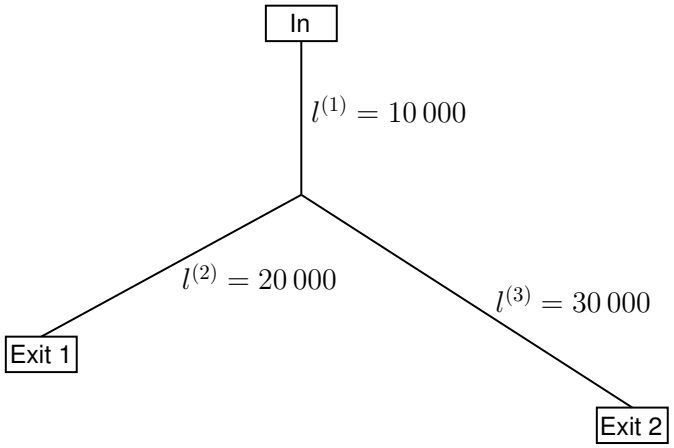


Figure 1: Sketch of a basic passive network.

**Example.** *Consider the internal node of the Y-shaped network depicted in Fig. 1. Here,* $n_L = \{1\}$, $n_R = \{2, 3\}$ *(sets of incoming/outgoing pipes) and consequently, the second component of* $\mathcal{T}$ *from pipe 1,* $\mathcal{T}_2^{(1)}$*, and the first component of* $\mathcal{T}$ *from pipe 2 and 3,* $\mathcal{T}_1^{(2)}$ *and* $\mathcal{T}_1^{(3)}$*, respectively, approach the junction. As a consequence, the original state variables* $\{(\rho^{(i)}, q^{(i)})\}_{i=1}^3$ *have to satisfy the linear system*

$$\begin{pmatrix} (2c_a)^{-1} & (2c_a a)^{-1} & 0 & 0 & 0 & 0 \\ 0 & 0 & (2c_a)^{-1} & (2c_a a)^{-1} & 0 & 0 \\ 0 & 0 & 0 & 0 & (2c_a)^{-1} & (2c_a a)^{-1} \\ 1 & 0 & -1 & 0 & 0 & 0 \\ 1 & 0 & 0 & 0 & -1 & 0 \\ 0 & 1 & 0 & -1 & 0 & -1 \end{pmatrix} \begin{pmatrix} \rho^{(1)} \\ q^{(1)} \\ \rho^{(2)} \\ q^{(2)} \\ \rho^{(3)} \\ q^{(3)} \end{pmatrix} = \begin{pmatrix} \mathcal{T}_2^{(1)} \\ \mathcal{T}_1^{(2)} \\ \mathcal{T}_1^{(3)} \\ 0 \\ 0 \\ 0 \end{pmatrix} \tag{19}$$

*at the junction, and* $\mathcal{T}_2^{(1)}, \mathcal{T}_1^{(2)}, \mathcal{T}_1^{(3)}$ *are obtained as linear combinations of the solution according to the transformation matrix* $L$*.*

Concerning the existence of broad solutions of (ISO 2) and their properties, we restrict ourselves to briefly recalling the results from [18]. Under certain conditions, we assume to be satisfied in the cases at hand, existence is established in Proposition 4 and Remark 1 of [18]. Further, the Lipschitz continuous dependency of the trace evaluation of $\rho$ on the friction coefficient $\lambda$ is proven in Proposition 6 of [18] where the latter result depends on Proposition 5 and Proposition 3 of the given reference. In particular, all of the given results also apply for passive networks of pipelines as discussed next.

## 2.3 Extension to passive networks

So far, the physical process of natural gas being transported is merely introduced on a single pipe. An extension to passive networks, represented as directed graph $G = (\mathcal{V}, \mathcal{E})$ with the notation of

Sect. 2.1, is obtained as follows. We restrict ourselves to tree networks with single entry (root of the tree), interior nodes (no consumption), and exit nodes assuming they are all leaves of the tree. Every edge $e \in \mathcal{E}$ models a pipe on its associated domain $(x_L^{(e)}, x_R^{(e)})$, where the transport equation (ISO 2) has to hold. In addition, for every node $k \in \mathcal{V}$, there exist index sets $n_L^k$, $n_R^k$ denoting its incoming and outgoing edges, respectively. Besides entry and exit nodes with assumed only one adjacent pipeline, i.e., $n_L^k$ is empty set, $n_R^k$ is singleton and vice versa, respectively, internal nodes connect at least two pipes, and thus, they correspond to points of pipe interaction. The type of such interactions is limited to junctions only, rendering the network passive in that no active elements like, e.g., compressors or valves are considered. As in the single-pipe scenario, entries and exits of the network require the definition of boundary conditions while, in order to obtain a well posed system of partial differential equations, initial conditions have to be introduced as well. In case of junctions, additional coupling conditions have to be imposed, characterizing the interplay of solutions to (ISO 2) on each of the adjacent pipes. On the one hand, the volume flow has to be balanced such that Kirchhoff's circuit law

$$\sum_{e \in n_L^k} q^{(e)}(x_R^{(e)}) + dq_k = \sum_{e \in n_R^k} q^{(e)}(x_L^{(e)}) \tag{20}$$

holds true. Here, $dq_k$ denotes possible injection or extraction of gas at the corresponding node. On the other hand, the pressure has to be conserved, i.e., we require

$$p^{(e)}(x_R^{(e)}) = p_k = p^{(e')}(x_L^{(e')}) \text{ for all } e \in n_L^k \text{ and } e' \in n_R^k. \tag{21}$$

As a consequence of the particular form (ISO-ALG) for steady states on single pipes, the representation of steady states for networks reduces to real numbers for every node and pipe where the numbers associated to pipes describe the constant volume flow along this element. This is due to the fact, that the data fixing the solution can be imposed at arbitrary position, and the numbers for the junctions describe pressure or density. The validation of feasibility of the solution now consist of checking the coupling conditions, and verifying, that the drop of density between two nodes can be described according to (ISO-ALG) along each pipe, i.e., if

$$\rho(x_L^{(e)})^2 - \rho(x_R^{(e)})^2 = 2\bar{\lambda}(x_R^{(e)})\tfrac{q^{(e)}|q^{(e)}|}{a^2}$$

holds for $e \in \mathcal{E}$. We immediately observe that in case of stationary solutions, the drop of density merely depends on $\bar{\lambda}(x_R^{(e)})$. Thus, instead of considering distributed frictions coefficients as in [13, 18], we restrict the discussion on pipe-wise constant coefficients $\lambda_e \in \mathbb{R}$, and thus, $\bar{\lambda}(x_R^{(e)}) = \lambda_e(x_R^{(e)} - x_L^{(e)})$ (cf. formula (7) Sect. 2.1). This is sufficient as we concentrate on a particular representative of all functions with the same integral value.

When considering networks of pipelines for gas transport in the time dependent setting, an important fact lies in the lack of observeability of distributed information along the pipes for a fixed point in time. On the one hand, this introduces the requirement of taking measurements of the state at a fixed spatial position like entry- or exit nodes for several times. On the other hand, it implies a lack of knowledge about the initial state within the pipes which is a more severe drawback. The structure of broad solutions as solution of ordinary differential equations with an initial condition depending on distributed information on the initial state of the system strictly requires corresponding knowledge. As in [7, 18], we assume the initial conditions of the time dependent PDE-problems to be given as steady states that can be computed efficiently (see, e.g. [19]).

# 3 Uncertainty quantification for the semilinear model

This section introduces the Bayesian approach to inverse problems, clarifies the involved probability distributions and provides an algorithm for sampling from the posterior distribution.

The Bayesian approach to inverse problems as, e.g., discussed in [2], is based on the following theorem.

**Theorem 2** (Bayes' Theorem)**.** *Assume that*

$$Z := \int_{\mathbb{R}^n} \pi_{DL}(y - \mathcal{G}(\lambda))\pi_{PR}(\lambda)d\lambda > 0. \tag{22}$$

*Then $\lambda|y$ is a random variable with Lebegue density $\pi_{PO}(\lambda)$ given by*

$$\pi_{PO}(\lambda) = \frac{1}{Z}\pi_{DL}(y - \mathcal{G}(\lambda))\pi_{PR}(\lambda).$$

The result is suited to finite dimensional problems, but similar principles hold in case of a function space setting, where merely a Radon-Nikodym density of measures associated to posterior and prior density is given (see [2] for details). In case of pipewise constant friction coefficients and a finite number of density measurements, the inverse problem renders finite dimensional in that input as well as observations are finite dimensional objects. However, we still have to consider solutions to the state system that are given in their associated function spaces.

Concerning the data likelihood we assume the measurement errors at each spatial position and time to be independent and identically distributed according to a normal distribution with mean zero and a variance of $0.001$.

Based on consultations with industry partners, the friction coefficients within a newly produced pipes can be assumed to be distributed according to a truncated normal distribution, i.e., a distribution that is derived from that of a normally distributed random variable by bounding it from above or below and a probability density function given as

$$\pi_{TN}(\lambda) = \frac{\phi\left(\frac{\lambda-\mu}{\sigma}\right)}{\sigma\left(\Phi\left(\frac{b-\mu}{\sigma}\right) - \Phi\left(\frac{a-\mu}{\sigma}\right)\right)}. \tag{23}$$

Here, $\phi$ and $\Phi$ denote the probability and cumulative density functions of the standard normal distribution, respectively, where $\mu = 0.018172$ and $\sigma = 0.0005$ are mean and variance. The truncation is set up by values $a^{new} = 0.01813$ and $b^{new} = 0.018206$ denoting the respective upper and lower bounds. While operating, the flow-performance of pipes worsens in that the friction coefficient increases. In order to incorporate this knowledge into the prior-modeling, we allow for an increased upper bound truncating the normal distribution in case of aged pipes, i.e., setting $b = 0.021$. The lower bound remains as before in this scenario as we do not expect the friction coefficient to drop in the aging process. Fig. 2 provides rescaled probability density function for both cases and demonstrates the increased domains of the probability density function, and thus, possible choices of $\lambda$.

The following result enables the usage of Theorem 2.

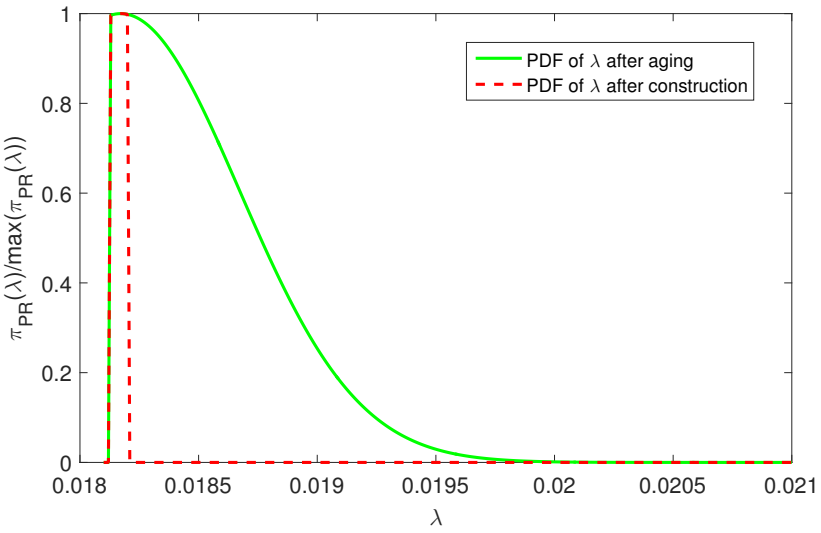


Figure 2: PDF for the truncated normal distribution .

**Proposition 1.** *The factor $Z$ as defined in* (22) *is strictly positive.*

*Proof.* As outlined above, the prior is assumed to be a truncated normal distribution on each of the pipes. Moreover, they are independently distributed providing

$$\pi_{PR}(\lambda) = \prod_{i=1}^{|\mathcal{E}|} \pi_{TN}(\lambda_i). \tag{24}$$

Here, $\pi_{TN}$ denotes the pdf of the probability distribution introduced in (23), $\lambda_i$ denotes the $i$-th component of the vector of friction coefficients and $|\mathcal{E}|$ the total number of pipes. In other words, the support of $\pi_{PR}$ and consequently $\pi_{PO}$ is compact. According to the results from Sect. 2.2, the observation operator $\mathcal{G}(\lambda)$ depends Lipschitz continuously on $\lambda$, and in addition, the probability density function $\pi_{DL}$ is a continuous function rendering the concatenation

$$\lambda \mapsto \pi_{DL}(y - \mathcal{G}(\lambda)) \tag{25}$$

continuous. The celebrated Weierstrass' Theorem now guarantees the existence of a minimum for $\pi_{DL}(y-\mathcal{G}(\lambda))$ on the compact support of $\pi_{PR}$, denoted by $\underline{\pi}$. Moreover, since the support is bounded, this minimum has to be strictly positive. Consequently, we estimate

$$Z \geq \underline{\pi} \int_{\mathbb{R}^n} \pi_{PR}(\lambda) d\lambda > 0, \tag{26}$$

where the latter inequality holds by properties of the truncated normal distribution. □

The Markov chain Monte Carlo method is designed to generate a Markov chain with associated stationary distribution that equals $P(\lambda|y)$. The main advantage lies in avoiding the computation of $Z$ given

in (22). This quantity is expensive to compute as it usually requires the application of Monte Carlo methods as well. Thus, we apply a method merely working with ratios of different posterior distribution, ensuring this factor to be canceled out. The respective algorithm is called Metropolis Hastings algorithm and defined next.

**Data:** Proposal density $\pi(\lambda'|\lambda)$, measured data $y$.
Initialization, i.e., choose $\lambda^{(0)} \in \mathbb{R}^{N_P}$, set $i = 0$.
Compute $\bar{\pi}_{PO}(\lambda^{(0)}) := \pi_{DL}(y - \mathcal{G}(\lambda^{(0)}))\pi_{PR}(\lambda^{(0)})$.
**for** $i \geq 0$ **do**
Draw proposed friction coefficient $\lambda'$ from proposal density $\pi(\cdot|\lambda_{(i)})$.
Compute

$$\alpha = \min\left\{1, \frac{\bar{\pi}_{PO}(\lambda')\pi(\lambda'|\lambda^{(i)})}{\bar{\pi}_{PO}(\lambda^{(i)})\pi(\lambda_{(i)}|\lambda')}\right\}. \tag{27}$$

Set $\lambda^{(i+1)} = \lambda'$ with probability $\alpha$ and $\lambda^{(i+1)} = \lambda^{(i)}$ with probability $1 - \alpha$.
**end**

**Algorithm 1:** Metropolis Hastings Algorithm

# 4 Numerical Realization

Within this section, two major points are pursued. On the one hand, the numerical realization of solving the coupled systems of time dependent partial differential equations is described. On the other hand, a set of examples for the method is provided and put into context with different approaches for gaining statistics and choices for the measurement positions.

Concerning the discretization of the state systems, we employ a numerical scheme that is based on piecewise constant averages of the state functions and also utilized in [13, 18]. These cell averages are computed on a uniform grid dividing pipes into $N$ cells of width $\Delta x$, which are referred to as internal cells. The boundary and coupling conditions at entry and exit nodes and junctions are realized by ghost cells, i.e., each pipe has a ghost cell on both ends as depicted in Fig. 3.

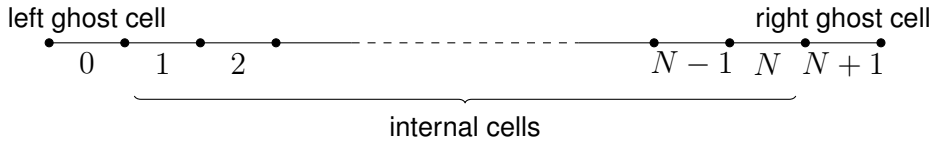


Figure 3: Spatial discretization of a pipe whit ghost cells

The scheme is inspired by the particle method from [8] that is consistent with entropy solutions of scalar conservation laws and that was already used for semilinear systems of conservation laws in [14, 15]. Note that the special structure of Eigenvalues for the differential operator under consideration renders the method more structures than initially intended, as it can be interpreted on a uniform grid. At time step $n$ an explicit Euler method is used to approximate the solutions to (18) for each component of the

transformed variables, i.e., for the first characteristic,

$$\mathcal{T}_1(y_{i-1}^{n+1}) = \mathcal{T}_1(y_i^n) + \tfrac{\Delta t}{c_a a}\lambda_i \tfrac{q_i^n|q_i^n|}{\rho_i^n},$$

and for $\mathcal{T}_2$, respectively. For equidistantly distributed particles with distance $\Delta x$, a time step $\Delta t = a^{-1}\Delta x$ and integral averages $y_i^n$ and $\lambda_i$, the original state variables can be reconstructed by $L\mathcal{T}(y)$, yielding the discretization scheme

$$\begin{aligned}
\rho_i^{n+1} &= \tfrac{1}{2}(\rho_{i+1}^n + \rho_{i-1}^n) - \tfrac{c_{CFL}}{2}(q_{i+1}^n - q_{i-1}^n) - \tfrac{\Delta t}{2a}\left(\lambda_{i-1}\tfrac{q_{i-1}^n|q_{i-1}^n|}{\rho_{i-1}^n} - \lambda_{i+1}\tfrac{q_{i+1}^n|q_{i+1}^n|}{\rho_{i+1}^n}\right),\\
q_i^{n+1} &= \tfrac{1}{2}(q_{i+1}^n + q_{i-1}^n) - \tfrac{a^2 c_{CFL}}{2}(\rho_{i+1}^n - \rho_{i-1}^n) - \tfrac{\Delta t}{2}\left(\lambda_{i-1}\tfrac{q_{i-1}^n|q_{i-1}^n|}{\rho_{i-1}^n} + \lambda_{i+1}\tfrac{q_{i+1}^n|q_{i+1}^n|}{\rho_{i+1}^n}\right),
\end{aligned} \tag{28}$$

$i = 1, ..., N$, corresponding to the Lax-Friedrichs scheme, where $c_{CFL}$ refers to the Courant number.

The similarity of the particle method to a classical TVD discretization scheme, mirroring the nature of broad solutions by integrating along characteristic lines, suggests a procedure for obtaining the values of the state at the ghost cells by employing the concept of broad solutions in the following way. At entry or exit nodes of the network, the updated value for the state is obtained by evaluating the ingoing transformed variable and solving the linear systems defined by the matrices $C_L$ or $C_R$, respectively, i.e, to solve

$$C_L^{-1}\begin{pmatrix} \mathcal{T}_1(y_0^{n+1}) \\ d_0(t^{n+1}) \end{pmatrix} \text{ and } C_R^{-1}\begin{pmatrix} \mathcal{T}_2(y_{N+1}^{n+1}) \\ d_{N+1}(t^{n+1}) \end{pmatrix}$$

for boundary data $d_0, d_{N+1}$ on the left and right ghost cell, respectively. Explicitly, this provides

$$\begin{aligned}
\rho_{0/N+1}^{n+1} &= \rho_{1/N}^n \mp \tfrac{1}{a} q_{1/N}^n \pm \tfrac{1}{a} d_{0/N+1}(t^{n+1}) \pm \tfrac{\Delta t}{a}\lambda_{1/N}\tfrac{q_{1/N}^n|q_{1/N}^n|}{\rho_{1/N}^n},\\
q_{0/N+1}^{n+1} &= d_{0/N+1}(t^{n+1}).
\end{aligned} \tag{29}$$

At junctions, all ingoing transformed variables and the coupling conditions form linear systems that have to be solved for the values of the state variables on the corresponding ghost cells. In case of a junction with three pipes, the system is given as (19).

Summarizing, we have established an algebraic expression that provides the updated state at all ghost cells $g$ of the network, based on the current iterate and the boundary conditions at the next time step $d(t^{n+1})$, i.e., $(\rho_g^{n+1}, q_g^{n+1}) = f_g(\rho^n, q^n, \lambda, d(t^{n+1}))$.

In general, the linear systems that have to be solved to determine the values of the states at the ghost cells are very small and constant over time. As a consequence, the most effective way to compute the associated solutions is given by precomputing the inverse matrices once and using them to compute the values on the ghost cells directly.

Since we consider steady states in the initial conditions of the systems, we employ the closed form solutions of them, depending merely on the current value of the friction coefficient. The associated cell averages can be computed exactly from this closed forms.

In the following numerical experiments we utilized a mesh width of $\Delta x = 10$ and fixed the speed of sound to $a = 300$. Moreover, we considered a time horizon of $T = 200$ when solving the underlying

system of partial differential equations and utilized a varying volume flow at the entry node of the corresponding networks given by

$$q(t, x_{In}) = 300 + 20 * sin((2\pi/50)t),$$

while the volume flow at the exit nodes is set constant, equaling the initial value of the volume flow in the adjacent pipe.

## 4.1 Discussion of numerical examples

In this section we are going to discuss two different network examples in order to illustrate the results of Algorithm 1 in particular situations. The first example is taken from Sect. 2.2, while the second example considers a slightly larger network.

#### Example 1

This example compares results from the Markov chain Monte Carlo approach presented in the work at hand and the statistical approaches for the example considered in [18]. The experimental setup consists of a plain network depicted in Fig. 1 with three pipelines, connected via a single junction. Artificial data have been generated by solving the underlying problem for the friction coefficient

$$\lambda_N = (0.018172, 0.018195, 0.018145)^\top$$

on a fine discretization with associated initial data, providing a reference solution $(\bar{\rho}, \bar{q})$. Here, the pipes are numbered counter-clock wise, beginning with the pipe at the entry node. In [18], an inverse problem for identifying the friction coefficient from noisy measurements was studied. To obtain statistical information on the results, the noise in the measurements was generated several times and the corresponding identification problems

$$\begin{aligned}
&\text{minimize} \frac{1}{2}\Big(\sum_{i=0}^{20}(\rho(10\cdot i, x_{E_1}) - \rho^d_{E_1}(10\cdot i))^2 + (\rho(10\cdot i, x_{E_2}) - \rho^d_{E_2}(10\cdot i))^2\Big) + \tfrac{\alpha}{2}\|\lambda - \lambda_M\|^2_{l^2}\\
&\text{subject to} (\rho^{(i)}, q^{(i)}) = \mathcal{S}(\lambda^{(i)}) \text{ on } (0,T)\times(x_L^{(i)}, x_R^{(i)}),\\
&\qquad (\rho^{(i)}(0,x), q^{(i)}(0,x)) \text{ solves (ISO-ALG) with given } q_0^{(i)} \text{ for } \lambda^{(i)},\\
&\qquad \rho(t, x_R^{(1)}) = \rho(t, x_L^{(2)}) = \rho_L^{(3)}, \;\; q^{(1)}(t, x_R^{(1)}) = q^{(2)}(t, x_L^{(2)}) + q^{(3)}(t, x_L^{(3)}),\\
&\qquad q^{(1)}(t, x_L^{(1)}) = q^d_{In}(t), q^{(2)}(t, x_R^{(2)}) = q^d_{Exit_1}(t), q^{(3)}(t, x_R^{(3)}) = q^d_{Exit_2}(t),\\
&\qquad \rho^{(1)}(t, x_L^{(1)}) = 52.3,\\
&\qquad 10^{-9} \le \lambda^{(i)} \le \overline{\lambda},\\
&\quad \text{with} \rho^d_{E_1}(10\cdot i) = \bar{\rho}(10\cdot i, x_{E_1}) + \eta_i, \rho^d_{E_2}(10\cdot i) = \bar{\rho}(10\cdot i, x_{E_2}) + \mu_i
\end{aligned}$$

were solved for variables $\eta, \mu \in \mathbb{R}^{20}$ that are component wise i.i.d. with respect to $\mathcal{N}(0, 10^{-3})$. This corresponds to repeating the same experiment several times and resulted in

$$E^{Inverse}[\lambda] = (0.018105, 0.018288, 0.018284)^\top$$

with

$$C^{Inverse} = cov(\lambda_i, \lambda_j) = \begin{pmatrix} 0.030719 & -0.042635 & -0.063932 \\ -0.042635 & 0.059173 & 0.088732 \\ -0.063932 & 0.088732 & 0.133057 \end{pmatrix} \cdot 10^{-5}$$

for expected value and covariance matrix, respectively.

For the Bayesian approach, we utilized the same physical set up, i.e., we considered the Y-shaped network presented in Fig. 1 with the same initial values, in particular, $q = (300, 120, 180)^\top$ and $\rho(x_{Entry}) = 52.3$.

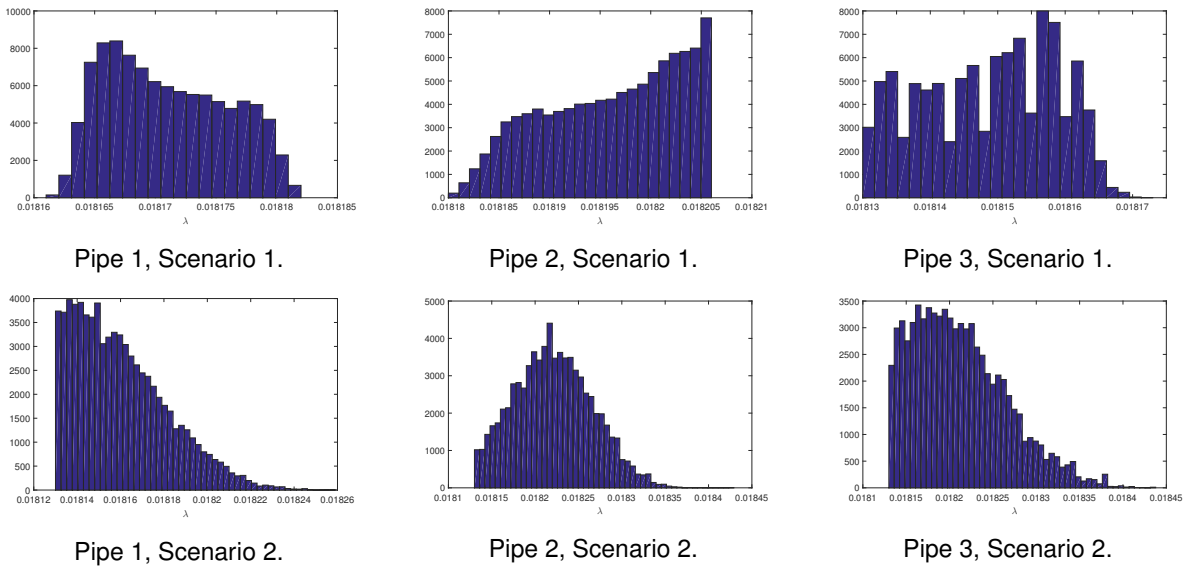

Pipe 1, Scenario 1. Pipe 2, Scenario 1. Pipe 3, Scenario 1.

Pipe 1, Scenario 2. Pipe 2, Scenario 2. Pipe 3, Scenario 2.

Figure 4: Histograms of the resulting trajectories of Algorithm 1 for scenarios 1 and 2.

To demonstrate the influence of certain parameters that determine the Bayesian approach for solving the inverse problem, we investigate different scenarios in the latter case. First, we considered data that are, similar to the identification problem, based on $\lambda_N$, i.e., we are considering 'new' pipes in that their friction coefficient is take from the interval $[0.01813, 0.018206]$. Here, we compare the influence of the chosen prior distribution and present results for both possibilities sketched in Fig. 2 referred to as scenario 1 and 2, respectively. In the considered scenarios, the expected values are given by

$$E^{Bayes_1}[\lambda] = (0.018171, 0.018196, 0.018149)^\top,$$
$$E^{Bayes_2}[\lambda] = (0.018160, 0.018221, 0.018212)^\top,$$

where the associated covariance matrices is of order $10^{-10}$ and $10^{-8}$, respectively. We refrain from presenting the full covariance matrices since in both examples the order of them is to small to influence the outcome in the numerical experiments of Sect. 5.2.

Fig. 4 provides histograms of the components of the Markov chain generated by Algorithm 1, and thus, it gives an idea of the associated probability density functions. Moreover, we provide the Markov chain for scenario 1 in Fig. 5.

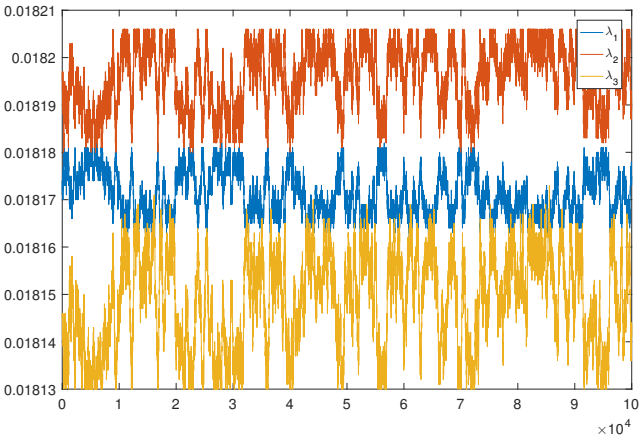


Figure 5: Trajectory generated in scenario 1.

Recall that the Bayesian approach is designed to gain information on the posterior probability density function, while the statistics based on the inverse problem from [18] can at most be considered as fair approximation. Thus, the difference in the results of both approaches is not suspicious as the latter method, e.g. does not incorporate prior knowledge on the distribution of $\lambda$ to the process. As it can be seen in the orders of the covariance matrices associated with scenario 1 and 2, the stochastic effect of the friction coefficient in freshly produced pipes is very small and has almost no influence on the problem of validating technical feasibility of stationary solutions for the underlying system under random demand.

However, to demonstrate, even when utilizing the Bayesian approach, that operating a network of pipelines introduces stochastic effects into problems as the validation problem, we in addition consider scenario 3 with the prior function for aged pipes and data that are generated with friction coefficients

$$\lambda_O = (0.02, 0.019, 0.0195)^\top,$$

i.e., we consider aged pipes where $\lambda$ became larger. In that situation, the results computed by Algorithm 1 turn out as

$$E^{Bayes_3}[\lambda] = (0.020244, 0.018660, 0.018977)^\top$$

and

$$C^{Bayes_3} = cov(\lambda_i, \lambda_j) = \begin{pmatrix} 0.030359 & -0.041560 & -0.061995 \\ -0.041560 & 0.058673 & 0.084921 \\ -0.061995 & 0.084921 & 0.130697 \end{pmatrix} \cdot 10^{-6}$$

for expected value and covariance matrix, respectively. In contrast to the previous scenarios, the order of the covariance matrix became larger, and thus, it also introduces effects to the probability level of feasibility sets (see Sect. 5.2). The histograms of the components of the Markov chain are depicted in Fig. 6. Here, we observe larger supports in all of them, compared with the previous histograms shown in Fig. 4.

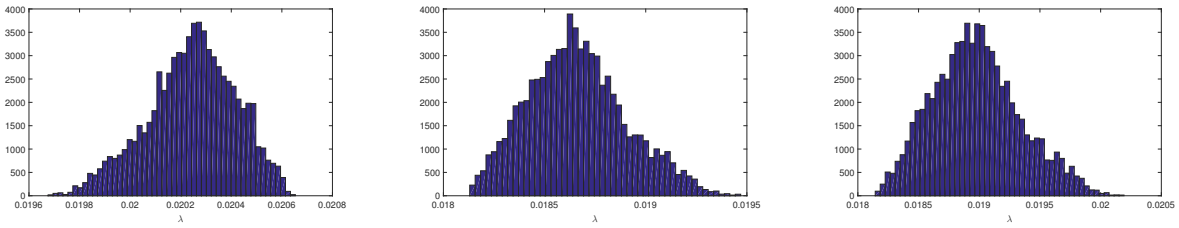


Pipe 1, Scenario 3. Pipe 2, Scenario 3. Pipe 3, Scenario 3.

Figure 6: Histograms of the resulting trajectories of Algorithm 1 for scenario 3.

In all considered cases, we observed a characteristic sign-structure in the covariance matrix that is implied by the network topology. The coupling and boundary conditions enforce low values of $\lambda$ in the pipes that are connected with the exit nodes, if the friction coefficient in the pipe connected to the entry node is large and vice versa, to compensate for density drops in the first pipe that are to large or to low, compared to the true solution.

**Example 2**

The second example aims on a larger network that is obtained by extending the network structure from Exampele 1 by further pipes as displayed in Fig. 7.

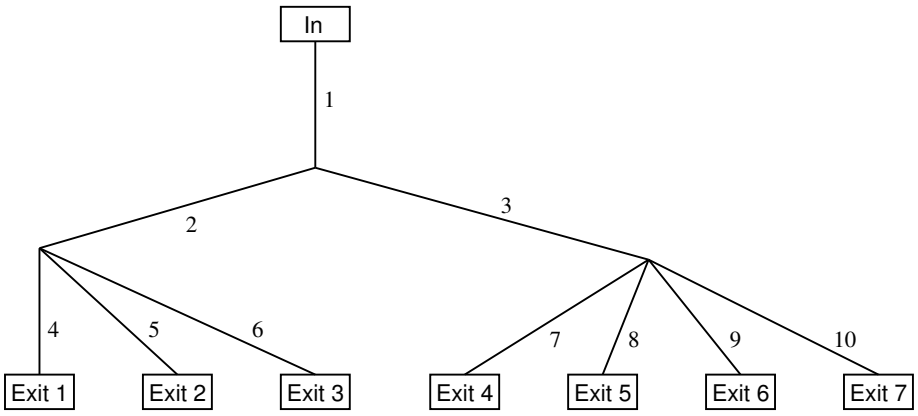


Figure 7: Sketch of the network from Example 2.

The network consist of $10$ pipes of length $7500$ with three interior, one entry and seven exit nodes. The

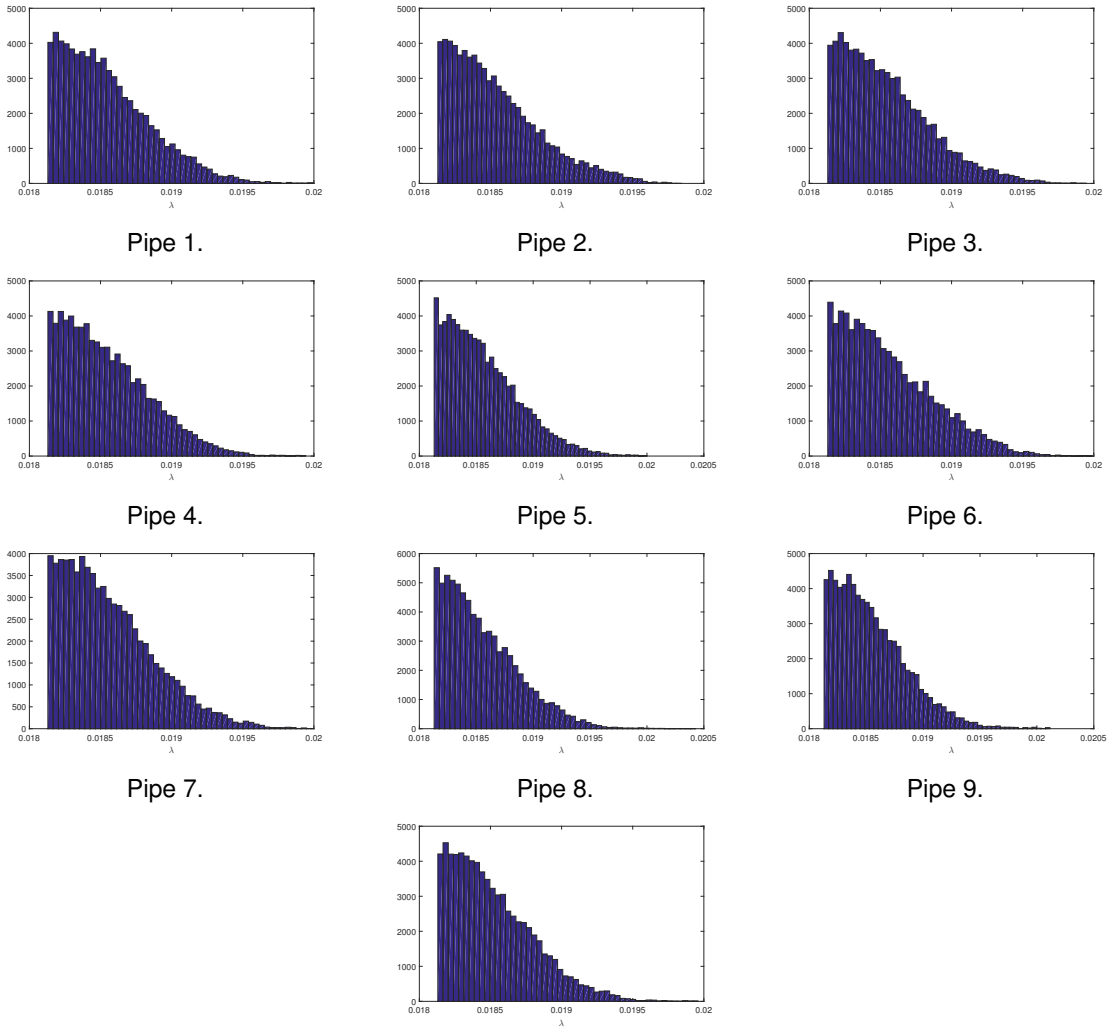

Pipe 1. Pipe 2. Pipe 3.

Pipe 4. Pipe 5. Pipe 6.

Pipe 7. Pipe 8. Pipe 9.

Pipe 10.

Figure 8: Histograms of the resulting trajectories from Algorithm 1 for Example 2

initial state is based on the pipewise constant volume flow

$$q = (300, 120, 180, 30, 40, 50, 30, 40, 50, 60)^\top$$

and $\rho(x_{Entry}) = 52.3$. Again, measurements of the density are taken at the exit nodes at merely $10$ points in time and compared to a perturbed reference solution generated on a fine mesh for the friction coefficients

$$\lambda_O = (1.8172, 1.8195, 1.8145, 1.82, 1.816, 1.818, 1.817, 1.8152, 1.8175, 1.8141)^\top \cdot 10^{-2}.$$

Compared to the setting of the previous example, we restrict ourselves only on scenario 2, i.e., obtaining information on newly produced pipes, but, with the prior density that also covers aged pipes. The results

of Algorithm 1 are given by the expected values

$$E[\lambda] = (1.8547, 1.8539, 1.8546, 1.8546, 1.8562, 1.8559, 1.8564, 1.8553, 1.8550, 1.8520)^\top \cdot 10^{-2}$$

and a covariance matrix of

$$cov(\lambda_i, \lambda_j) = 10^{-7} \cdot$$

$$\begin{pmatrix}
0.934 & -0.014 & 0.001 & -0.039 & -0.005 & 0.005 & 0.015 & -0.001 & 0.027 & -0.012 \\
-0.014 & 0.976 & 0.018 & 0.044 & 0.013 & 0.068 & 0.067 & 0.024 & -0.028 & -0.009 \\
0.001 & 0.018 & 0.948 & -0.036 & -0.046 & -0.009 & -0.030 & 0.000 & 0.042 & -0.003 \\
-0.039 & 0.044 & -0.036 & 0.910 & 0.015 & -0.002 & -0.001 & 0.038 & 0.001 & -0.030 \\
-0.005 & 0.013 & -0.046 & 0.015 & 1.026 & -0.013 & 0.034 & -0.040 & 0.018 & -0.023 \\
0.005 & 0.068 & -0.009 & -0.002 & -0.013 & 1.008 & -0.022 & -0.041 & -0.024 & 0.034 \\
0.015 & 0.067 & -0.030 & -0.001 & 0.034 & -0.022 & 1.007 & -0.043 & -0.022 & -0.021 \\
-0.001 & 0.024 & 0.000 & 0.038 & -0.040 & -0.041 & -0.043 & 1.043 & 0.000 & -0.017 \\
0.027 & -0.028 & 0.042 & 0.001 & 0.018 & -0.024 & -0.022 & 0.000 & 0.974 & 0.036 \\
-0.012 & -0.009 & -0.003 & -0.030 & -0.023 & 0.034 & -0.021 & -0.017 & 0.036 & 0.830
\end{pmatrix}$$

after $75000$ iterations. We observe, that due to the obviously increased network complexity, the structure of the network can no longer be derived from the sign structure of the covariance matrix. Moreover, the order of the covariance matrix is quite larger as before, even in scenario 2, and the expected value differs slightly from $\lambda_O$. In Fig. 8 we provide the histograms for the considered scenario.

# 5 Determining probabilities of feasibility sets

Next, the random nature of the exit load vector as well as the uncertainty of friction along the pipes is taken into account. For simplification, as before we want to restrict to a tree shaped gas transport network involving a single entry node (labeled with $0$) and a number of $n$ exit nodes. Further we assume that the network is in steady state (see Sect. 2.1). The aim of this section is the computation of the probability of the event that a random load (or demand) vector is technical feasible under uncertain friction in the sense of (16). Since the demand vector $(b_0, b)$ must be balanced, in the following we assume that $b_0 = -\mathbb{1}^\top b$, that is, the total exit demand can always be satisfied by the corresponding supply at the single entry node. By doing so, the following set of feasible pairs of exit load vectors and friction coefficients becomes relevant

$$\tilde{M}_{\text{feas}} := \left\{ (b, \lambda) \in \mathbb{R}^{n \times m} \mid g_{k,l}(b, \lambda) \geq 0;\ k, l = 0, \ldots, n;\ k \neq l \right\}, \tag{30}$$

where technical feasibility can be formulated by a set of constraint mappings $g_{k,l}(\cdot, \cdot)$ arriving in a natural way from (16). In particular, we have that

$$g_{k,l}(b, \lambda) := (p_k^{max})^2 + h_k(b, \lambda) - (p_l^{min})^2 - h_l(b, \lambda), \tag{31}$$

where $h_k(\cdot, \cdot)$ taken from (15), $k, l = 0, \ldots, n$ and $k \neq l$. More precisely, if $(b, \lambda)$ is identified with some random vector $\big(b(\omega), \lambda(\omega)\big)$ on a probability space $(\Omega, \mathcal{A}, \mathbb{P})$, then

$$\mathbb{P}\left\{ \omega \;\middle|\; \big(b(\omega), \lambda(\omega)\big) \in \tilde{M}_{\text{feas}} \right\} \tag{32}$$

marks the probability of exit demand vectors to be feasible in the context of uncertain friction. The main variation of exit load data is temperature driven. However, even at fixed temperature, considerable random variation remains. That is why exit loads can be understood as a stochastic process depending on temperature and may be characterized by a finite family of multivariate distributions, each of them referring to some (rather narrow) range of temperature and reflecting the joint distribution of loads at the given set of exit points, see [19, Chapter 13]. As recorded in the same reference [19, Table 13.3], these distributions are most likely to be Gaussian (possibly truncated) or lognormal. Our assumption to consider a multivariate Gaussian distribution for $b$ can therefore be seen as a prototype setting which maybe adapted without much effort to more realistic settings (multivariate log-normal distributions etc.). As well as the load vector the uncertainty of friction coefficients approximately follows a multivariate Gaussian distribution whose parameter can be estimated as seen before. Thus, we assume that

$$b \sim \mathcal{N}(\mu_1, \Sigma_1) \qquad \text{and} \qquad \lambda \sim \mathcal{N}(\mu_2, \Sigma_2), \tag{33}$$

where $\mu_1$, $\mu_2$ and $\Sigma_1$, $\Sigma_2$ denote mean values and covariance matrices of the demand and friction random vectors, respectively. Clearly, by formula (30) we could use the final inequality system in order to test feasibility of simulated outcomes of the pairs $(b, \lambda)$ according to the given Gaussian distributions. The average number of feasible simulations would yield the Monte Carlo estimate for the desired probability in (32). Such Monte Carlo approach has two drawbacks: first it may come up with a comparatively large variance for the obtained probability estimation and, second, it does not provide us with information about the sensitivity of this probability with respect to changes of external parameters, that could subject of optimization. This sensitivity (derivative) information is crucial, however, in order to set up any efficient algorithm of nonlinear optimization in order to solve optimization problems in the context of gas transmission, for example the maximization of booking capacities [16].

## 5.1 Spheric-radial decomposition

Instead of crude Monte Carlo sampling we rather propose here the so-called spheric-radial decomposition of Gaussian random vectors (see, e.g. [3, 9]). This alternative not only may significantly reduce the variance of probability estimations but, moreover, it offers the possibility of efficiently approximating gradients of (32) with respect to external network parameters. This last feature is of supreme importance for optimization problems under probabilistic constraints [23].

**Theorem 3.** *Let $(b, \lambda)$ be a Gaussian random vector distributed according to* (33)*. Then for the probability of random load and random friction being technical feasible it holds that*

$$\mathbb{P}\left((b,\lambda) \in \tilde{M}_{\text{feas}}\right) = \int\limits_{(v_1,v_2)\in\mathbb{S}^{n+m-1}} \mu_\chi \left\{ r \geq 0 \;\middle|\; (rL_1v_1 + \mu_1, rL_2v_2 + \mu_2) \in \tilde{M}_{\text{feas}} \right\} d\mu_\eta,$$

*where matrices $L_i$ are such that $\Sigma_i = L_i L_i^\top$ (e.g., Cholesky decomposition), $i = 1, 2$, and, $\mu_\chi$ is the law of chi-distribution with $n + m$ degrees of freedom and $\mu_\eta$ is the law of uniform distribution at the Euclidean unit sphere $\mathbb{S}^{n+m-1}$.*

In order to evaluate the integrand in the spheric integral above, for any fixed direction $(v_1, v_2) \in \mathbb{S}^{n+m-1}$, one has to be able to compute the $\chi$-probability of the one-dimensional set

$$\{r \geq 0 \,|\, (rL_1v_1 + \mu_1, rL_2v_2 + \mu_2) \in \tilde{M}_{\text{feas}}\}.$$

Thus, using (30) computing the probability of feasibility amounts to characterizing the set

$$\{r \geq 0 \,|\, g(rL_1v_1 + \mu_1, rL_2v_2 + \mu_2) \geq 0\} \qquad (v \in \mathbb{S}^{n+m-1}), \tag{34}$$

where we define

$$g(b, \lambda) := \min_{\substack{k,l=0,\dots,m \\ k \neq l}} \left\{ (p_k^{\max})^2 + h_k(b, \lambda) - (p_l^{\min})^2 - h_l(b, \lambda) \right\}. \tag{35}$$

Applying the idea of spheric-radial decomposition presented in Theorem 3, we propose the following algorithm for computing the probability $\mathbb{P}\big((b, \lambda) \in \tilde{M}_{\text{feas}}\big)$.

**Data:** Let be $(b, \lambda)$ random vector according to (33).
Set $S = 0$ and sample $N$ points $\{v^1, \dots, v^N\}$ uniformly distributed on the sphere $\mathbb{S}^{n+m-1}$.
**for** $i = 1, \dots, N$ **do**
  Find the zero's of the one dimensional function
  $\theta(r) := g(rL_1v_1^i + \mu_1, rL_2v_2^i + \mu_2)$
  with $g$ defined in (35) and represent the set
  $M^i := \{r \geq 0 \,|\, \theta(r) \geq 0\}$
  corresponding to (34) as a disjoint union of intervals
  $M^i = \cup_{j=1}^{s} [\alpha_j, \beta_j]$,
  where $\alpha_j, \beta_j$ are the zero's obtained before and ordered appropriately.
  Compute the $\chi$-probability of $M^i$ according to
  $\mu_\chi(M^i) = \sum_j F_\chi(\beta_j) - F_\chi(\alpha_j)$,
  where $F_\chi$ refers to the cumulative distribution function of the one-dimensional
  $\chi$-distribution with $n + m$ degrees of freedom.
  Put $S := S + \mu_\chi(M^i)$.
**end**
Set $\mathbb{P}\big((b, \lambda) \in \tilde{M}_{\text{feas}}\big) := S/N$.

**Algorithm 2:** Spheric-radial decomposition

A few words on this algorithm are in order at this place. The algorithm clearly provides an approximation to the spheric integral in Theorem 3 by means of a finite sum based on sampling of the sphere, and then, averaging the values of the integrand over all samples. Of course, this approximation will improve with the sampling size which may be large depending on the dimension $n + m$ of the problem (i.e., exit nodes and edges in the network) and on the desired precision for the probability.

We recall that the uniform distribution on the sphere $\mathbb{S}^{n+m-1}$ can be represented as the distribution of $\eta/\|\eta\|$ (Euclidean norm), where $\eta$ has a standard Gaussian distribution in $\mathbb{R}^{n+m}$, i.e., $\eta \sim \mathcal{N}(0, I)$. Then, the simplest idea to sample points $v^i$ on the sphere would be to independently sample $m + n$ values $w_j$ of a one-dimensional standard normal distribution by using standard random generators and

then putting $v^i := w/\|w\|$ for $w := (w_1, \ldots, w_{n+m})$. When replacing such Monte Carlo sampling of the normal distribution (based on random number generators) by Quasi-Monte Carlo sampling (based on deterministic low discrepancy sequences), one observes a dramatic improvement in the precision of the result. For the problem of nomination validation in gas networks (with fixed friction coefficients), this was revealed in [11].

## 5.2 Preliminary numerical results

A considerably numerical study with respect to computations of probabilities of technical feasibility in stationary networks under stochastic exit demand can be found in [11]. However, the impact of uncertainty of friction along the pipes to the probability level of feasible exit load situation has not been investigated so far. Therefore, the aim of the numerical study in this paper is to incorporate the effect of random friction into the consideration in [11]. For our numerical tests we proceed with the two example networks already discussed in Sect. 4.1. Even if we consider tree shaped networks only, the results can easily transferred to more complex situation involving cycles within the network topology.

**Example 1**

For the purpose of illustration we start with the small network serving as example for computing the probability of feasibility as in (32). The network consists of one entry node, one passive (interior) node and two exit nodes, where we consider a stochastic gas demand. The shape of the network is given by Fig. 1. Observe, that the passive node can be formally modeled as an exit node, but, with zero consumption. As there exist 3 arcs joining the nodes, we have three frictional driven roughness coefficients $\Lambda_e = 2a^2 l_e \lambda_e$, where $e = 1, 2, 3$ (cf. (6)).

We like to mention here that this example network already was considered in [10], where a numerical study of the influence of uncertain friction (roughness) is provided. But, compared to the propose of this paper, no distribution information for friction is used. Instead, a complete robust approach for describing uncertainty with respect to friction along the pipes is applied.

| Mean $\mu_1$ | Covariance $\Sigma_1$ |
|---|---|
| $(120.0, 180.0)$ | $\begin{pmatrix} 1\,600.0 & 800.0 \\ 800.0 & 4\,000.0 \end{pmatrix}$ |

| Node | Pressure $p^{min}$ | Pressure $p^{max}$ |
|---|---|---|
| Entry | $40.0$ | $52.0$ |
| Interior | $40.0$ | $52.0$ |
| Exit 1 | $40.0$ | $52.0$ |
| Exit 2 | $40.0$ | $52.0$ |

Table 1: Distribution for the exit demand and network parameters of Example 1.

In this paper we are going to base the computations directly on the distribution information of friction estimated by the Markov chain Monte Carlo method in Sect. 4.1. Because the variance with respect to the friction coefficients in case of new pipes turn out to be too small, we provide the computations for Example 1 only for the results of Algorithm 1 when considering aged pipes. In particular, for the

multivariate Gaussian friction coefficient $\lambda \sim (\mu_2, \Sigma_2)$ the mean value is set to $\mu_2 = E^{Bayes_3}[\lambda]$ with corresponding covariance matrix $\Sigma_2 = C^{Bayes_3}$ (see Sect. 4.1, Example 1). The length of the pipes is set to $l = (10\,000, 20\,000, 30\,000)$.

In addition, the parameter for the bivariate Gaussian distributed exit demand vector $b \sim \mathcal{N}(\mu_1, \Sigma_1)$ as well as the fixed network parameters are displayed in Table 1. The pressure limits are given in bar, whereas the exit demand is given in volume flow (as before). Note that exit demand is frequently given in thermal power $P$ instead of mass or volume flow $q$ by network owners . However, the relation between thermal power and mass flow is given by the equation $P = qH_c$, where $H_c$ refers to the calorific value of the gas.

In order to study how the stochastic behavior of friction affects technical feasibility, we performed a test series to compute the probability of feasibility under stochastic exit demand. In particular, we compare different random friction situation by randomly chosen samples simulated from the distribution. In addition, we compare the results with the computations that we obtain when using a) the friction mean value $\mu_2$ b) the friction mean value plus standard deviation $\mu_2 + \sigma_2$ and c) the friction mean value minus standard deviation $\mu_2 - \sigma_2$, in order to incorporate the friction part according to (35). Finally, we determine the probability of technical feasibility in a full stochastic environment, i.e., where we assume that both friction and exit load follow the stated multivariate Gaussian distributions. Table 2 summarizes

| Samples | Random scenarios | | | Reference scenarios | | | Full stochastic |
|---|---|---|---|---|---|---|---|
| | $\lambda_{[1]}$ | $\lambda_{[2]}$ | $\lambda_{[3]}$ | $\mu_2$ | $\mu_2 + \sigma_2$ | $\mu_2 - \sigma_2$ | $\mathcal{N}(\mu_2, \Sigma_2)$ |
| $1\,000$ | 70.417 | 68.917 | 69.227 | 69.699 | 68.787 | 70.620 | 69.694 |
| $5\,000$ | 70.320 | 68.816 | 69.126 | 69.600 | 68.685 | 70.524 | 69.521 |
| $10\,000$ | 70.319 | 68.818 | 69.127 | 69.601 | 68.688 | 70.522 | 69.549 |
| $50\,000$ | 70.301 | 68.792 | 69.103 | 69.579 | 68.662 | 70.504 | 69.580 |
| $100\,000$ | 70.297 | 68.789 | 69.100 | 69.575 | 68.659 | 70.500 | 69.580 |

Table 2: Numerical results, related to Example 1, in order to study the impact of uncertain friction to the technical feasibility. The table compares the probabilities of the obtained feasibility sets in different situations with respect to friction, computed via spheric-radial decomposition.

the numerical results. All computations were performed by Algorithm 2. The number of samples on the unique sphere varies between $1\,000$ and $100\,000$ samples. Clearly, the accuracy increases with a higher number of samples on the sphere used for the approximation. However, we obtain a notable effect of using different random outcomes for the friction coefficients (column 2 to 4). We obtain a variation by the computed probability levels of about 2 percent compared to the average value of nearly 70 percent (column 5). On the other hand, in that example problem we realize that a fully stochastic approach for both friction and load distribution (last column) does not return a significant difference in contrast to proceeding with stochastic exit demand and the mean value for friction. Considering the small network, we conclude that a accurate approximation of the mean value for the friction part seems to be sufficient for a quite fair approximation of the probability level of feasibility sets with respect to random exit demand.

**Example 2**

Now we discuss Example 2 from Sect. 4.1. The underlying network can be viewed as enlargement of the network in Example 1 by adding additional pipes end nodes to the net as illustrated in Fig. 7. We base our computations directly on the estimated data from Sect. 4.1 (Example 2) for the friction coefficients. In a different way from Example 1 the following numerical results are related to non-aged pipes. However, for the computations we proceed in almost the same manner as before. The length of pipes we slightly enlarge to $l_e = 10\,000$ for all involved pipes $e = 1, \ldots, 10$. The Gaussian distribution for the friction comes up with the Markov chain Monte Carlo estimation by mean $\mu_2 = E[\lambda]$ and by covariance $\Sigma_2 = cov(\lambda_i, \lambda_j)$ (see Sect. 4.1, Example 2). All additional parameters, in particular, the assumed Gaussian distribution for the exit demand are displayed by Table 3.

| Mean $\mu_1$ | Covariance $\Sigma_1$ |
|---|---|
| $\begin{pmatrix} 30.0 \\ 40.0 \\ 50.0 \\ 30.0 \\ 40.0 \\ 50.0 \\ 60.0 \end{pmatrix}$ | $\begin{pmatrix} 64.0 & 8.0 & 32.0 & -16.0 & 8.0 & -16.0 & 16.0 \\ 8.0 & 82.0 & 31.0 & 7.0 & 19.0 & -29.0 & -7.0 \\ 32.0 & 31.0 & 146.0 & -16.0 & -23.0 & 5.0 & 16.0 \\ -16.0 & 7.0 & -16.0 & 42.0 & 15.0 & -7.0 & 0.0 \\ 8.0 & 19.0 & -23.0 & 15.0 & 99.0 & 20.0 & 17.0 \\ -16.0 & -29.0 & 5.0 & -7.0 & 20.0 & 98.0 & 0.0 \\ 16.0 & -7.0 & 16.0 & 0.0 & 17.0 & 0.0 & 112.0 \end{pmatrix}$ |

| Node | Pressure $p^{min}$ | Pressure $p^{max}$ |
|---|---|---|
| Entry | $45.0$ | $52.0$ |
| Interior 1–3 | $45.0$ | $52.0$ |
| Exit 1–7 | $45.0$ | $52.0$ |

Table 3: Distribution for the exit demand and network parameters of Example 2.

As in Example 1, the considered test series aim to approximate the probability of feasibility under stochastic exit demand in different situation with respect to friction. Again, the computations include three randomly selected friction samples simulated from the distribution, results that are obtained when using the friction mean value $\mu_2$, the friction mean value plus standard deviation $\mu_2+\sigma_2$, and the friction mean value minus standard deviation $\mu_2 - \sigma_2$. As well as considering these fixed friction vectors we determine the probability of technical feasibility in a fully stochastic environment once more, i.e., where we assume that both friction and exit load follow the given multivariate Gaussian distributions.

Table 4 shows the very similar results of all computations, but, for Example 2 now. As before, applying randomly selected friction coefficients obviously guides to a falsified estimation of the probability of feasibility. Only a proper estimation of the average friction can serve as a good base for accurate computation. Nevertheless, in the environment of the enlarged network topology also the calculation wit the mean value differs slightly from the fully stochastic result. Using the mean value seems to overestimate the probability level compared with the stochastic approach. The latter observation gives a hint to what happens when taking more involved networks with a much higher number of pipes and

| Samples | Random scenarios | | | Reference scenarios | | | Full stochastic |
|---|---|---|---|---|---|---|---|
| | $\lambda_{[1]}$ | $\lambda_{[2]}$ | $\lambda_{[3]}$ | $\mu_2$ | $\mu_2 + \sigma_2$ | $\mu_2 - \sigma_2$ | $\mathcal{N}(\mu_2, \Sigma_2)$ |
| $1\,000$ | 93.140 | 95.015 | 91.574 | 93.376 | 91.950 | 94.629 | 93.429 |
| $5\,000$ | 93.309 | 95.121 | 91.780 | 93.534 | 92.146 | 94.748 | 93.513 |
| $10\,000$ | 93.211 | 95.053 | 91.667 | 93.439 | 92.036 | 94.673 | 93.449 |
| $50\,000$ | 93.268 | 95.061 | 91.768 | 93.489 | 92.126 | 94.690 | 93.430 |
| $100\,000$ | 93.252 | 95.049 | 91.749 | 93.473 | 92.107 | 94.677 | 93.417 |

Table 4: Numerical results, related to Example 2, in order to study the impact of uncertain friction to the technical feasibility. The table compares the probabilities of the obtained feasibility sets in different situations with respect to friction, computed via spheric-radial decomposition.

nodes into the consideration. In such a case we expect that the usage of expected friction only causes a to optimistic overestimation of the probability level for the feasibility of random exit demand.

# References

[1] A. Bressan. *Hyperbolic systems of conservation laws*, volume 20 of *Oxford Lecture Series in Mathematics and its Applications*. Oxford University Press, Oxford, 2000. The one-dimensional Cauchy problem.

[2] M. Dashti and A. M. Stuart. *The Bayesian Approach to Inverse Problems*, pages 311–428. Springer International Publishing, 2017.

[3] I. Déak. Subroutines for computing normal probabilities of sets-computer experiences. *Annals of Operations Research*, 100:103–122, 2000.

[4] T. J. Dodwell, C. Ketelsen, R. Scheichl, and A. L. Teckentrup. A hierarchical multilevel Markov chain Monte Carlo algorithm with applications to uncertainty quantification in subsurface flow. *SIAM/ASA J. Uncertain. Quantif.*, 3(1):1075–1108, 2015.

[5] P. Domschke. *Adjoint-Based Control of Model and Discretization Errors for Gas Transport in Networked Pipelines*. PhD thesis, TU Darmstadt, 2011.

[6] P. Domschke, B. Hiller, J. Lang, and C. Tischendorf. Modellierung von Gasnetzwerken: Eine Übersicht. Technical Report 2717, Technische Universität Darmstadt, 2017.

[7] H. Egger, T. Kugler, and N. Strogies. Parameter identification in a semilinear hyperbolic system. *Inverse Problems*, 33(5):055022, 25, 2017.

[8] Y Farjoun and B. Seibold. Solving one dimensional scalar conservation laws by particle management. *Meshfree methods for partial differential equations IV*, 65:95, 2008.

[9] A. Genz and F. Bretz. *Computation of multivariate normal and t-probabilities*, volume 195 of *Lecture Notes in Statistics*. Springer, Heidelberg, 2009.

[10] T. González Grandón, H. Heitsch, and R. Henrion. A joint model of probabilistic/robust constraints for gas transport management in stationary networks. *Computational Management Science*, 14:443–460, 2017.

[11] C. Gotzes, H. Heitsch, R. Henrion, and R. Schultz. Feasibility of nominations in stationary gas networks with random load. *Mathematical Methods of Operations Research*, 84:427–457, 2016.

[12] M. Gugat, M. Herty, and V. Schleper. Flow control in gas networks: exact controllability to a given demand. *Math. Methods Appl. Sci.*, 34(7):745–757, 2011.

[13] S. Hajian, M. Hintermüller, C. Schillings, and N. Strogies. A Bayesian approach for parameter identification in gas networks. Technical report, WIAS Berlin, 2018. Preprint.

[14] F. M. Hante. *Hybrid Dynamics Comprising Modes Governed by Partial Differential Equations: Modeling, Analysis and Control for Semilinear Hyperbolic Systems in One Space Dimension*. PhD thesis, University Erlangen-Nuremberg, 2010.

[15] F. M. Hante and G. Leugering. Optimal boundary control of convention-reaction transport systems with binary control functions. In *HSCC*, pages 209–222. Springer, 2009.

[16] H. Heitsch. On probabilistic capacity maximization in a stationary gas network. Technical report, WIAS Berlin, 2018. Preprint.

[17] M. Herty, J. Mohring, and V. Sachers. A new model for gas flow in pipe networks. *Math. Methods Appl. Sci.*, 33(7):845–855, 2010.

[18] M. Hintermüller and N. Strogies. On the identification of the friction coefficient in a semilinear system for gas transport through a network. Technical report, WIAS Berlin, 2018. Preprint, Submitted.

[19] T. Koch, B. Hiller, M. E. Pfetsch, and L. Schewe, editors. *Evaluating gas network capacities*, volume 21 of *MOS-SIAM Series on Optimization*. Society for Industrial and Applied Mathematics (SIAM), Philadelphia, PA, 2015.

[20] R. J. LeVeque. *Finite volume methods for hyperbolic problems*. Cambridge Texts in Applied Mathematics. Cambridge University Press, Cambridge, 2002.

[21] B. L. Rožděstvenskiĭ and N. N. Janenko. *Systems of quasilinear equations and their applications to gas dynamics*, volume 55 of *Translations of Mathematical Monographs*. American Mathematical Society, Providence, RI, 1983. Translated from the second Russian edition by J. R. Schulenberger.

[22] J. Stolwijk and V. Mehrmann. Error analysis and model adaptivity for flows in gas networks. *Analele Stiintifice Univ. Ovidius Constanta. Seria Matematica*, 2017. Accepted for publication.

[23] W. v. Ackooij and R. Henrion. (Sub-) gradient formulae for probability functions of random inequality systems under Gaussian distribution. *SIAM/ASA Journal on Uncertainty Quantification*, 5:63–87, 2017.